Materials Horizons

ROYAL SOCIETY OF CHEMISTRY

COMMUNICATION

Published on 21 October 2026
Licensed under CC-BY 4.0

Check for updates

Cite this: DOI: 10.1039/d6mh01719c

Received 13th August 2026,
Accepted 21st October 2026

DOI: 10.1039/d6mh01719c

rsc.li/materials-horizons

Closing the perovskite loop: aqueous recovery and reuse of $MAPbI_3$ for film, device, and nanocrystal reuse

Zhaoyi Du,[a] Ding Ding,[b] Longren Li,[b] Weitao Qian,[a] Enny Tran,[ab] Milo S. P. Shaffer,[ab] Artem A. Bakulin,[b] Nicola Gasparini[b] and Martyn A. McLachlan *[a]

The rapid commercialisation of organic–inorganic metal halide perovskites (MHPs) presents significant end-of-life challenges, particularly owing to the environmental and health risks their lead content poses. Despite efforts to improve perovskite device performance, comparatively little attention has been given to safe and sustainable recycling, with reported approaches being reliant on hazardous solvents, including DMF. Here, we report the development and use of a water-based solvent for the selective recovery of methylammonium lead iodide ($MAPbI_3$) from MHP devices. The solvent comprises of water with low concentrations of dissolved malic acid, β-alanine, and sodium iodide (NaI), in which the organic additives enable $MAPbI_3$ dissolution and NaI supports direct MHP recovery. Owing to the temperature dependent solubility of $MAPbI_3$ in our solvent, high-purity powders can be recovered through precipitation by solvent cooling. Films fabricated from recycled $MAPbI_3$ exhibit microstructures and bandgaps comparable to those prepared from pristine $MAPbI_3$, whilst recycled films show improved morphological uniformity and reduced non-radiative recombination. In photoconductor devices, recycled $MAPbI_3$ films deliver a higher photocurrent density, 1.48×10^{-5} A cm^{-2}, and lower dark current density, 1.25×10^{-7} A cm^{-2} compared to their pristine analogues. When incorporated into p–i–n photovoltaic devices, recycled $MAPbI_3$ films retain >90% of the efficiency of pristine devices. Furthermore, demonstrating the versatility of the solvent system beyond thin-film reuse, $MAPbI_3$ recovered from thin films is successfully repurposed for the preparation of perovskite nanocrystals. Overall, this work establishes a green and efficient route for the recovery, recycling, and reuse of metal halide perovskites (MHPs), supporting a more circular lifecycle for emerging perovskite optoelectronics.

New concepts

Closing the perovskite loop: aqueous recovery and reuse of $MAPbI_3$ for film, device, and nanocrystal reuse.

This work introduces a fully aqueous, green solvent system for the selective recovery, recycling, and functional reuse of methylammonium lead iodide ($MAPbI_3$) from metal halide perovskite thin-film devices – establishing a closed-loop recycling strategy that avoids the hazardous organic solvents that underpin virtually all existing approaches. While prior recycling efforts have demonstrated lead capture or component recovery, none have achieved a complete loop in which recovered material is reprocessed into devices that surpass the performance of their pristine counterparts. This counterintuitive outcome combined with superior morphological uniformity, reduced non-radiative recombination, and enhanced photoconductor metrics in recycled devices arises from preformed perovskite species in solution that promote more controlled crystallisation, a mechanistic insight with broader implications for perovskite film deposition strategies. The additional demonstration that recovered $MAPbI_3$ can be repurposed into luminescent nanocrystals further establishes the versatility and circularity of the platform. This work reframes recycling not as a remediation step, but as a route to functional enhancement, offering the materials community a sustainable, scalable, and low-cost pathway toward truly circular perovskite optoelectronics.

1. Introduction

Metal halide perovskites (MHPs) have emerged as a versatile class of semiconductors with broad potential spanning diverse optoelectronic applications. The rapid development of MHPs has been driven largely by their promise in photovoltaics (PVs), light-emitting diodes (LEDs) and photodetectors (PDs).[1–3] Increasingly, their attractive photophysical and electronic properties are also being exploited in more diverse technologies, including lasers, sensors, and photocatalytic systems.[4–6] In the PV sector there has been rapid progress towards commercialisation,[7–9] with imaging, display and PD technologies rapidly nearing commercialisation.[10–12] The expansion of research activity and commercial interest in MHPs has made the development of effective end-of-life capture and recycling strategies a priority. This is critical from the perspective of resource efficiency and

[a] Department of Materials, Molecular Sciences Research Hub, Imperial College London, London, W12 0BZ, UK
[b] Department of Chemistry, Molecular Sciences Research Hub, Imperial College London, London, W12 0BZ, UK. E-mail: martyn.mclachlan@imperial.ac.uk

broader sustainability and owing to the presence of lead. In humans, lead can adversely affect the central nervous, reproductive, developmental, cardiovascular and immune systems and when released is environmentally persistent.[13,14] Innovative, highly effective recycling strategies have evolved whereby layer-by-layer dissolution of PVs have been developed,[15] although current recycling strategies often depend on organic solvents for dissolution.[16] Such solvents are critical for the deposition of MHP films and in post-deposition defect reduction.[17,18] However, they also carry inherent toxicity and environmental concerns.[19,20] This further refines the requirements for emerging capture and recycling strategies, emphasising that consideration must extend beyond recovery performance to the nature of the materials used in the process and the risks they may pose to human health and the environment. Remarkably this is an area that remains relatively unexplored, despite growing interest in end-of-life management of MHP materials and devices. Early attention focussed on the recycling of the hazardous and high-value PV components, with substrate/transparent conducting oxide recovery achieved through a multi-step lead capture process and subsequent reuse.[20] More recently aqueous-based recycling strategies have begun to emerge, whereby multiple functional components are combined holistically to recover and regenerate MHP PVs. Taken together, these studies highlight both the promise of aqueous recycling and the fact that it remains underdeveloped relative to the broader maturity and scale of perovskite device research.

Recently we demonstrated an aqueous solvent system capable of supporting the size-controlled synthesis of MHP nanocrystals, yielding materials with excellent photon-to-electron conversion in simple photoconductor architectures.[21] The solvent comprises water with low concentrations of dissolved malic acid and β-alanine where the synergistic interaction between malic acid and β-alanine promotes adduct formation with $PbBr_2$, overcoming its otherwise poor aqueous solubility and enabling subsequent precipitation of the desired MHP phase. Here, we demonstrate the recovery and reuse of the MHP active layer using an optimised aqueous solvent system. Our aqueous solvent system dissolves the metal halide perovskite (MHP) layer, enabling direct capture and recovery of α-phase $MAPbI_3$ in its original perovskite form – rather than as a decomposed precursor. This represents a key distinction from many existing perovskite recycling approaches, which typically recover only the lead halide salt (PbX_2). Those that have demonstrated perovskite recovery do so use a series of organic solvents.[22] In very recent work $MAPbI_3$ recovery has been demonstrated using an acidic solution with additives that afford control of solubility, phase purity and stability.[23] Table S1 benchmarks our approach against prior reports, comparing perovskite composition, solvent system, dissolution/recovery strategy, recovery efficiency, and post-recycling device performance.

Our recovered $MAPbI_3$ is reprocessed *via* conventional routes to produce perovskite nanocrystals (PNCs) and thin films that, upon integration into photoconductor and PV devices, deliver performance metrics comparable to their pristine analogues. We further demonstrate the versatility of the process by converting recovered MHP films into emissive PNCs. Our aqueous solvent system provides an effective route for MHP recovery and subsequent reuse, enabling repurpose as functional thin films or luminescent nanocrystals.

2. Results and discussion

Structural and morphological characterisation of dissolution and reprecipitation

Process optimisation was carried out using films $MAPbI_3$, 400 nm thickness, deposited onto glass substrates in a one-step deposition (see methods). In contact with water, $MAPbI_3$ typically undergoes hydration followed by irreversible degradation, forming soluble methylammonium and iodide species and insoluble PbI_2 (Fig. S1). A distinct visual modification of the substrate is observed as the film dissolves in our aqueous solution composed of malic acid, β-alanine and H_2O, changing from the characteristic black colour of $MAPbI_3$ to the transparent appearance of glass (Fig. S1). No precipitation is observed, the insoluble PbI_2 is solubilised through adduct formation with malic acid, confirmed using UV-vis absorption spectroscopy shown in Fig. S2. The spectra show an absorption peak centred at 293 nm, attributed to $PbI_2(Sol)_4$ iodoplumbates (where Sol is the aqueous solvent), confirming that molecular PbI_2 remains.[24] There is a small and broad absorption centred at 360 nm that is attributed to PbI_4^{2-}.[25]

β-alanine deprotonates the malic acid forming carboxylate groups that, in-turn interact with the insoluble PbI_2 to form a soluble adduct, Fig. 1a. ^{1}H NMR was conducted on DL-malic acid and on a DL-malic acid/β-alanine mixture, using D_2O as the solvent (Fig. S3). The methine proton (–C**H**(OH)–) peak of pure DL-malic acid centred at 4.56 ppm, shifting upfield to 4.33 ppm following addition of β-alanine. This upfield shift reflects increased electron shielding, consistent with the formation of carboxylate groups and thus deprotonation of malic acid. To further verify that the dissolution of PbI_2 is facilitated by protonated carboxylate groups in malic acid, we replaced β-alanine with NaOH (pK_b values >3 and <1 respectively). Again, the absorption spectra confirm the presence of $PbI_2(Sol)_4$ iodoplumbates with the lower energy peak not observed, Fig. S4, attributed to the strong base favouring complete deprotonation of the malic acid and the formation of a single product, $PbI_2(Sol)_4$.

The solubility of $MAPbI_3$ in the aqueous solvent is highly temperature dependent, Fig. S5, making cooling a convenient route to induce precipitation. In the absence of NaI, cooling produced a yellow precipitate and yellow suspension, consistent with PbI_2 formation, Fig. 1b. The addition of NaI to the solvent had no discernible effect on the dissolution process but significantly altered the nature of the solid recovered upon cooling. The precipitates were isolated by centrifugation, the supernatant removed, and the solids were washed with HI/IPA (see methods) before drying at 60 °C overnight in ambient air, following which X-ray diffraction (XRD) was performed, Fig. 1b. The yellow powder recovered was confirmed as PbI_2, with characteristic reflections at 12.77°, 25.59°, and 38.76° 2θ,

 This journal is © The Royal Society of Chemistry 2026

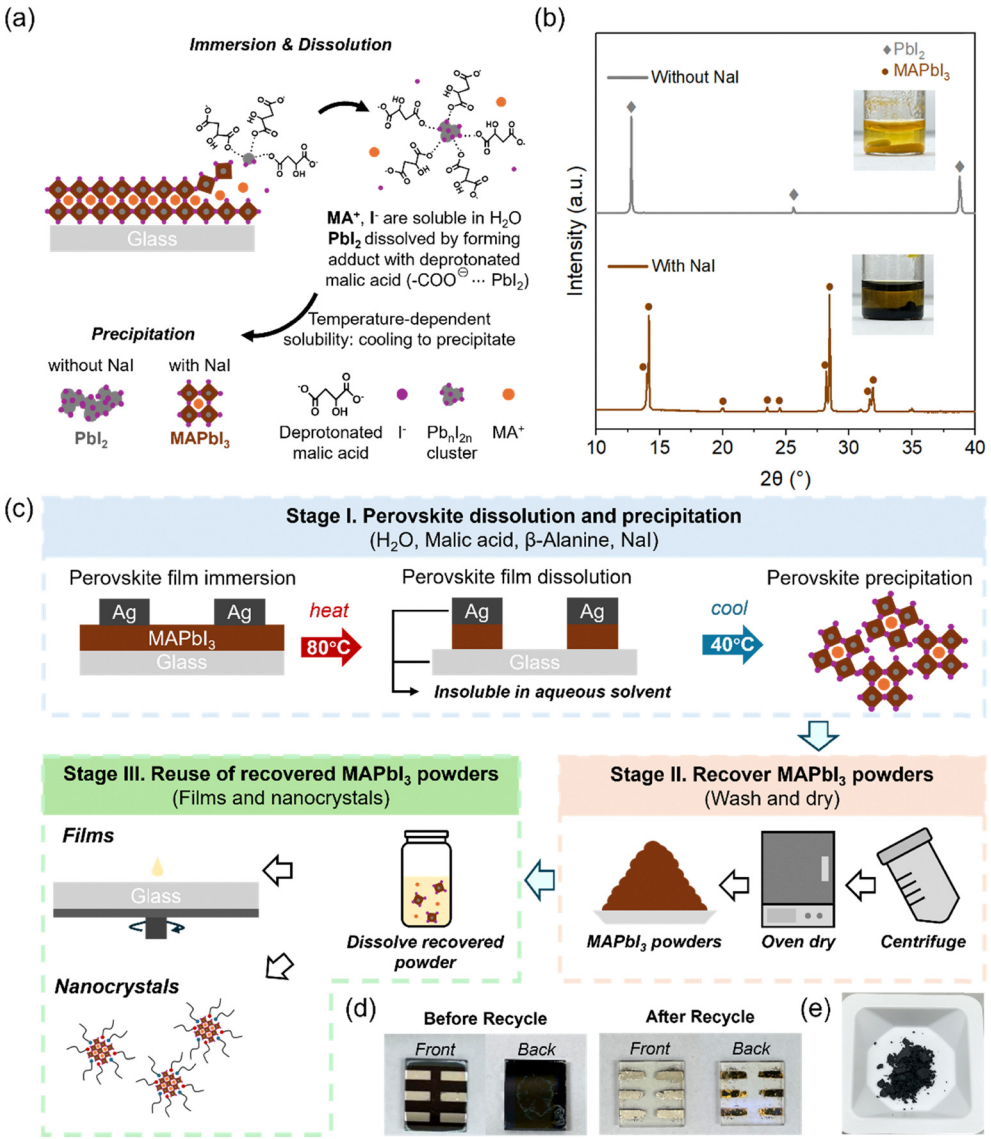


Fig. 1 (a) Schematic illustration of $MAPbI_3$ film dissolution and subsequent precipitation using the aqueous solvent system. (b) X-ray diffraction patterns of the solids recovered in the presence and absence of NaI – inset photographs show the corresponding precipitates in their respective solutions. (c) Schematic overview of the complete $MAPbI_3$ recovery, recycling and reuse process. (d) Photographs of photoconductor devices before and after removal and recovery of the $MAPbI_3$ layer. (e) Photograph of the recovered and dried $MAPbI_3$ powder.

assigned to the (001), (002), and (003) planes of hexagonal PbI_2 respectively.[26] In contrast, the powder recovered from the solvent containing NaI exhibited a diffraction pattern characteristic of $MAPbI_3$. Reflections at 14.02° and 14.15° 2θ are assigned to the (002) and (110) planes of tetragonal $MAPbI_3$ with the *I*4/*mcm* space group,[27] additional peaks at 28.17° and 28.48° 2θ correspond to the (004) and (220) planes respectively (ICSD 01-085-5507). These results demonstrate that the aqueous solvent system dissolves $MAPbI_3$ from the substrate and that NaI addition enables recovery of $MAPbI_3$, rather than decomposition to PbI_2.

To determine the role of NaI, UV-vis measurements were carried out on aqueous solvent systems containing: (i) $MAPbI_3$ without NaI, (ii) $MAPbI_3$ with NaI, and (iii) NaI without $MAPbI_3$, as shown in Fig. S6. Distinct differences are seen in the spectra in the 340–380 nm range, solution (i) shows no peaks in this range, whereas solutions (ii) and (iii) show peaks 370 and 358 nm respectively. The peak in solution (i) is attributed to the presence of PbI_3^-,[28] anticipated in iodide-rich conditions where PbI_2 can form a range iodoplumbates, *e.g.* PbI_3^-, PbI_4^{2-}.[29,30] Solution (iii) shows an absorption peak at 358 nm, originating from I_3^-.[31] The additional iodide anions present in the solutions containing NaI drive the formation of lead species with increased iodide coordination *i.e.* PbI_4^{2-}, PbI_5^{3-}, PbI_6^{4-} putting the lead into an octahedral coordination that readily results in the formation of $MAPbI_3$.[32]

ATR-FTIR and Raman spectroscopy were conducted to investigate further the dissolution/reprecipitation mechanism and the role of NaI. In the ATR-FTIR spectra, the band at 1710 cm^{-1}, assigned to ν(C═O) of –COOH groups, decreases in intensity

upon dissolution of $MAPbI_3$ and addition of NaI. The characteristic asymmetric and symmetric COO^- stretching bands, located at 1630 and 1385 cm^{-1} in the aqueous solvent, shift to 1626 and 1378 cm^{-1} after $MAPbI_3$ dissolution, indicating interactions between $MAPbI_3$ and the organic molecules. Upon addition of NaI, the asymmetric COO^- band shifts markedly to lower wavenumber, overlapping with adjacent bands to form a broad feature centred at 1573 cm^{-1}. This pronounced shift is consistent with the reported formation of Pb–carboxylate interactions.[33] Raman spectroscopy was conducted on the $MAPbI_3$ film and on $MAPbI_3$ dissolved in our solvent with and without NaI (Fig. S8), the peak positions given in Table S2. The low-wavenumber region (50–150 cm^{-1}) is assigned to vibrations of the Pb–I cage in $MAPbI_3$ and PbI_2, while the higher-wavenumber region (175–450 cm^{-1}) is typically assigned to methylammonium-related vibrations in $MAPbI_3$.[34] The $MAPbI_3$ film shows a series of peaks in the higher-wavenumber region that disappear following dissolution, indicating a loss of the the 3-D $MAPbI_3$ structure. In the solvent without NaI, three sharp, well-resolved peaks are observed at 61.3, 86.5 and 106.1 cm^{-1} *i.e.* in the low-wavenumber region, assigned to mixed I–Pb–I bending and Pb–I stretching modes, respectively.[35–37] Such sharp, PbI_2-like features have been attributed to perovskite decomposition.[38] In the presence of NaI, these Pb–I peaks broaden and shift to higher wavenumber, an additional peak around 136.5 cm^{-1} also appears, assigned to the antisymmetric I–I stretch of distorted I_3^-.[39] The broadening is consistent with a distribution of Pb–I coordination environments, rather than solely PbI_2. The increased iodide concentration will favour the formation of iodide-rich iodoplumbate species, potentially including $[[PbI_4]^{2-}$ and $[PbI_5]^{3-}$,[39] consistent with the UV-vis spectra, Fig. S6. Such species may preserve high Pb–I coordination during dissolution, thereby facilitating subsequent reconstruction of the PbI_6 framework during $MAPbI_3$ recovery.[34,39,40]

Assessment of lead recovery

Having demonstrated the dissolution and re-precipitation of $MAPbI_3$ in our aqueous solvent, we next assess the feasibility of recovering $MAPbI_3$ directly from perovskite devices. For this, we use a simple photoconductor with the structure glass/$MAPbI_3$/Ag, Fig. 1c. Devices were immersed in the aqueous solvent at 80 °C, resulting in dissolution of the black $MAPbI_3$ film, exposing the underlying substrate while leaving the electrodes intact, Fig. 1d. The selectivity of the aqueous solvent toward other materials commonly encountered in perovskite devices was also investigated. Hole transport layers (NiO_x) and electron transport layers (SnO_2), deposited as films on ITO-coated glass, were immersed in the aqueous solvent for 3 minutes. Analysis, Fig. S9, confirms that neither is soluble in our solvent, indicating selectivity towards the perovskite layer. Subsequent cooling of the resulting solution <40 °C induced $MAPbI_3$ precipitation, which was then separated, washed, and dried to yield $MAPbI_3$ powder, Fig. 1e. Following removal of the $MAPbI_3$ the solution was used to capture fresh $MAPbI_3$, and this dissolve–precipitate–separate cycle was repeated over multiple rounds. After each round, recovery yield was determined as:

$$\text{Recovery yield} = \frac{\text{recovered mass}}{\text{initial mass}} \times 100\%$$

Fig. S10 compares the recovery yield obtained using freshly prepared aqueous solvent against solvent that had already been reused following precipitate removal. Notably, solubility never falls to zero, thus a portion of the Pb that is solubilised on the first solvent use is retained. On subsequent rounds of reuse the recovered quantity matches the difference in solubility shown in Fig. S10 where the recovery yield is $>80\%$.

Building on the recovery yield evaluation, we further compared the toxicity of our aqueous solvent against organic solvents and water, Table S3. Organic solvents including DMF, DMSO, and GBL can cause serious health effects under prolonged exposure, whereas malic acid and β-alanine, the key components of our solvent, show no appreciable acute toxicity at the concentrations used here. NaI is present at a comparatively high concentration, as an iodine-rich environment is essential for stabilising the α-phase of $MAPbI_3$ during recovery; while this raises some toxicity concern, it remains substantially lower than that of the organic solvents. Pure water, by contrast, is essentially non-hazardous, but its use alone yields PbI_2, reducing the recovery efficiency.[41]

Reuse of recovered $MAPbI_3$

When the precipitate is removed the solvent can again be further reused, outlined schematically in Fig. 1c. The recovered $MAPbI_3$ was subsequently dissolved in DMF: DMSO (see methods) and spin-coated to glass substrates creating recycled films. Their structure was compared with pristine films prepared by conventional one-step deposition using XRD, Fig. 2a. The diffraction patterns are largely similar, with peaks consistent with tetragonal $MAPbI_3$ (ICSD 01-085-5507) with no discernible differences in peak position or relative intensity between the samples. A weak peak at approximately 12.6° 2θ is observed in the recycled film, indicating a small quantity of PbI_2. Given the structural similarity between the films, their optical bandgaps were determined by UV-vis spectroscopy and corresponding Tauc analysis, Fig. 2b. The extracted bandgaps are within experimental error of one another, at approximately 1.61 eV, consistent with reported values for $MAPbI_3$.[42]

The comparable structural and optical properties motivated further comparison of the film surface chemistry using X-ray photoelectron spectroscopy (XPS). Survey spectra, Fig. S11a, confirm the presence of Pb, I, N and C in both pristine and recycled films, with no additional elements detected following the dissolution-recrystallisation process. Closer inspection of the high-resolution C 1s spectra (Fig. S11b) reveals three components centred at 284.8, 286.3 and 287.6 eV, assigned to adventitious C–C/C–H, methylammonium carbon (with possible overlap from C–O species),[43,44] and surface carbonyl (C═O) species, respectively. Compared with the pristine film, the

 This journal is © The Royal Society of Chemistry 2026

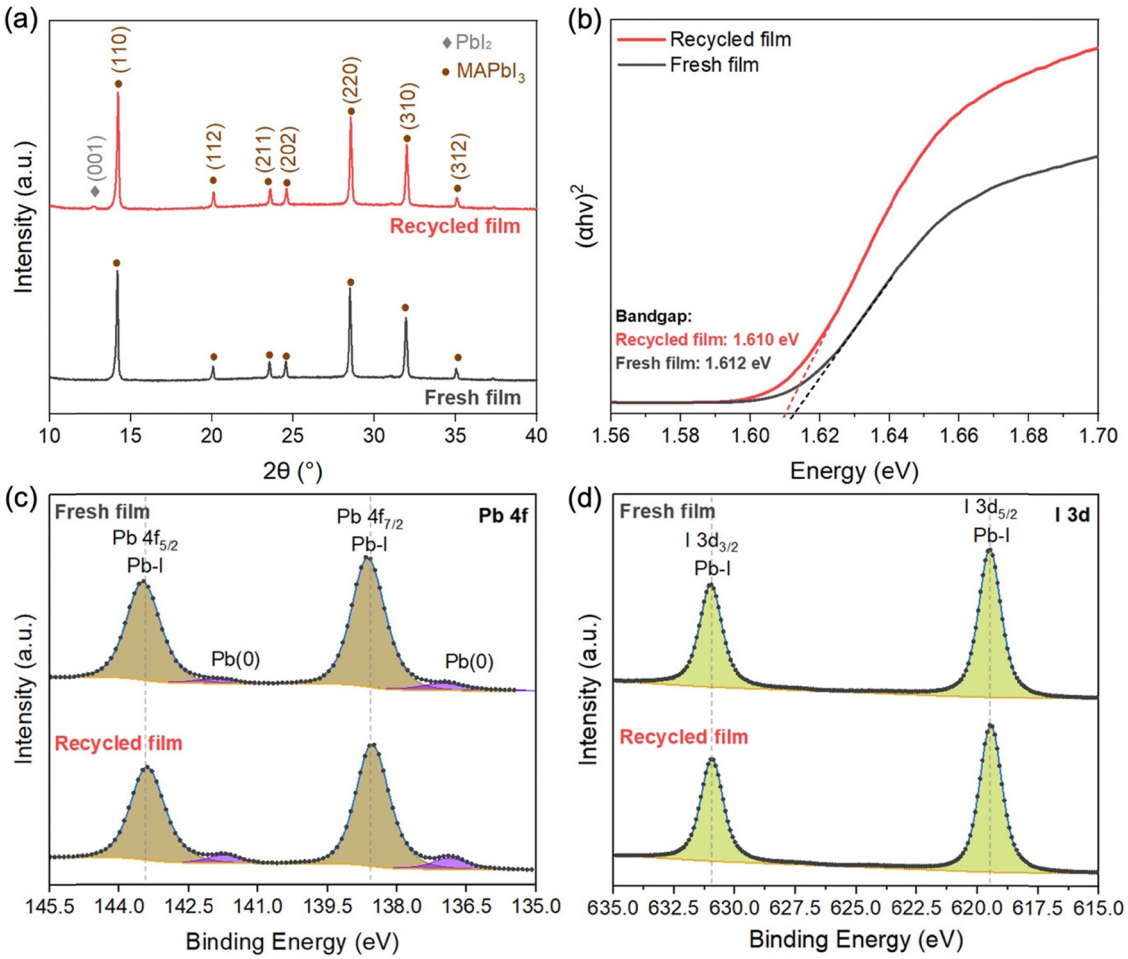


Fig. 2 Comparison of the structural, optical and chemical properties of pristine and recycled $MAPbI_3$ films: (a) X-ray diffraction patterns. (b) Tauc plots and high-resolution XPS spectra of the (c) Pb 4f and (d) I 3d regions.

overall fitted C–N/C–O component in the recycled sample exhibits a slight shift (~0.2 eV) toward higher binding energy, accompanied by a small increase in relative intensity. This is attributed to an increase in the relative contribution of C–O with respect to C–N. As these two signals overlap significantly in the XPS spectra and given that C–O typically appears at a slightly higher binding energy than C–N, a greater C–O contribution naturally manifests as an apparent shift toward higher binding energy. The elevated C–O contribution likely originates from oxygen-containing functional groups present in the organic molecules, malic acid and/or β-alanine. The Pb 4f and I 3d spectra also show a high degree of similarity, Fig. 2c and d. For both films, the Pb 4f spectrum is dominated by the characteristic Pb^{2+} doublet, with the Pb $4f_{7/2}$ and Pb $4f_{5/2}$ peaks centred at 138.6 and 143.4 eV, respectively, while the I $3d_{5/2}$ and I $3d_{3/2}$ peaks are located at 619.4 and 630.9 eV, with all binding energies falling within the range of reported values for $MAPbI_3$.[45–47] These observations indicate that a Pb–I bonding environment comparable to that of pristine material is reestablished after recycling. In addition to the Pb^{2+} doublet, weak metallic Pb^0 components are observed at approximately 136.9 eV and 141.8 eV in both the pristine and recycled films, arising from X-ray-induced reduction during measurement. As undercoordinated surface Pb is known to be particularly susceptible to such reduction,[48,49] the comparatively higher relative intensity of the metallic Pb^0 component suggests that the recovered $MAPbI_3$ exhibits reduced MAI passivation at the surface, most likely a consequence of preferential MAI dissolution during the IPA washing step of the recycling process.[50]

The surface morphology and thickness of the fresh and recycled films were analysed using scanning electron microscopy (SEM), Fig. 3a. Both films show a similar, compact polycrystalline structure, anticipated for MHP films, and are of comparable thickness. Analysis of the grain size distribution, Fig. S12, shows that the recycled films have subtly increased grain sizes and a narrower distribution. This increase in grain size and improved film uniformity may arise from the pre-formed ABX_3 perovskite structure of the recycled material. Following dissolution in DMF/DMSO and subsequent deposition, these pre-existing perovskite species likely alter the crystallisation pathway relative to fresh precursor solutions, promoting the formation of more compact and uniform films.[51]

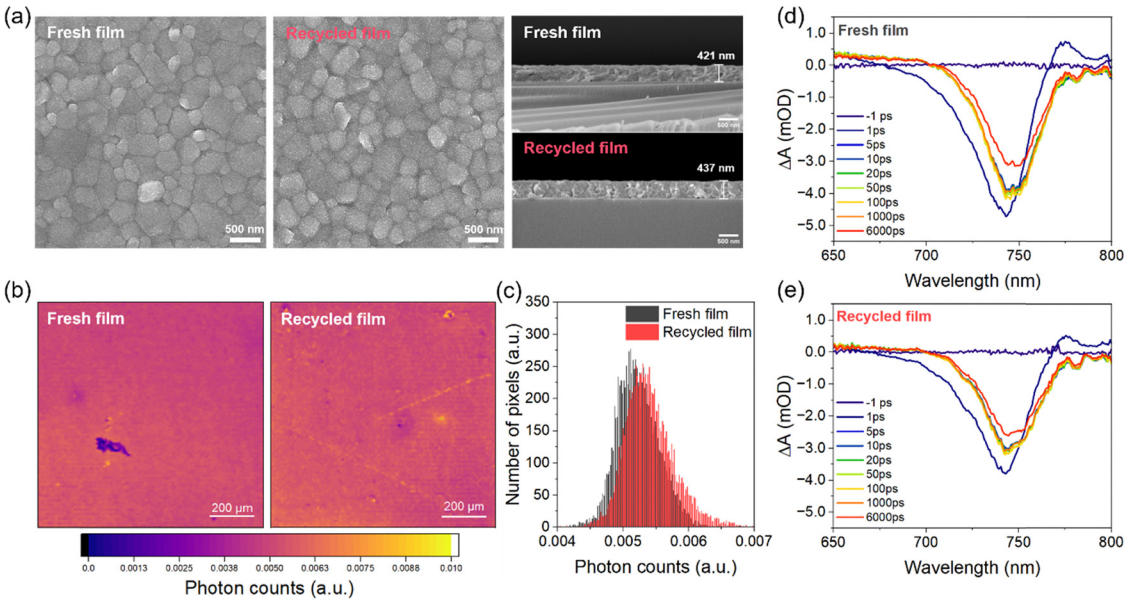


Fig. 3 Comparison of fresh and recycled $MAPbI_3$ films and photoconductor devices. (a) Top-view and cross-sectional SEM images. (b) Spatially resolved photoluminescence (PL) intensity maps and (c) corresponding photon-count distributions. Transient absorption (TA) spectra of (d) fresh and (e) recycled $MAPbI_3$ films at selected pump–probe delays following 400 nm excitation at a pump fluence of 0.4 μJ cm^{-2}.

Spectroscopic characterisation

Steady-state photoluminescence (PL) spectra of fresh and recycled films showed peaks at 772 nm and 770 nm respectively, Fig. S13. Spatially resolved PL mapping was also carried out on fresh and recycled films, Fig. 3b. Both show largely homogeneous PL intensity distributions across the mapped areas, indicating good macroscopic film uniformity. Under identical excitation and acquisition conditions, the recycled film shows a slightly higher mean PL intensity than the fresh film, Fig. 3c. This enhanced PL response is consistent with reduced non-radiative recombination, which is commonly associated with trap-mediated losses at surfaces and grain boundaries.[52] The spatially uniform PL response of the recycled film is also consistent with its compact morphology observed by SEM, Fig. 3a, and its narrower grain-size distribution, Fig. S12, together supporting improved microstructural uniformity.[53]

To assess whether the recycling process alters the photoexcited carrier dynamics of $MAPbI_3$, we performed femtosecond transient absorption (TA) spectroscopy on fresh and recycled films deposited on glass substrates, Fig. 3d and e. Upon photoexcitation, both samples display a pronounced negative band-edge bleach at ~730–750 nm, primarily attributed to photoinduced state filling, together with weaker broadband photoinduced absorption (PIA) features across 550–700 nm. Crucially, the fresh and recycled films exhibit highly similar spectral profiles and temporal evolution. No new transient features or shifts in the band-edge bleach are observed after recycling. Taken together, these observations suggest that the recycling process preserves the band-edge electronic structure and dominant relaxation pathways of $MAPbI_3$.

To further assess the carrier dynamics, we analysed the normalised band-edge bleach kinetics extracted at 750 nm, Fig. S14. Two distinct temporal regimes are evident. The initial sub-picosecond evolution is associated with rapid carrier thermalisation and cooling towards the band edge, together with the establishment of the band-edge carrier population. As these early-time processes are sensitive to local energetic disorder and local defects, the closely matched sub-picosecond dynamics suggest that recycling does not appreciably alter the local carrier-relaxation environment. This is followed by a much slower decay extending into the nanosecond regime, reflecting carrier recombination influenced by long-lived defect states. The long-time dynamics are therefore sensitive to recombination-active trap states, particularly deep traps that contribute to long-lived carrier decay. The close agreement between the fresh and recycled films across both temporal regimes indicates that the dominant carrier-cooling and recombination pathways remain largely unchanged after recycling.

Time-correlated single photon counting (TCSPC) measurements under 467 nm excitation were performed to provide complementary information on the carrier dynamics (Fig. S15). The biexponential fitting parameters are summarized in Table S4. The recycled perovskite film presents comparable lifetime (18.7 ns) to fresh perovskite films (16.8 ns). The modest increase in lifetime observed in the recycled film originates predominantly from a redistribution of the decay-component amplitudes rather than a systematic increase in the individual time constants. Specifically, the relative amplitude of the long-lived component increases from 0.22 to 0.28, whilst that of the short-lived component decreases from 0.78 to 0.72, the corresponding time constants remain comparable between the two samples. Together with the film morphology and PL mapping results, this modest increase in PL lifetime is consistent with reduced non-radiative recombination in the recycled

 This journal is © The Royal Society of Chemistry 2026

film, The TA measurements indicate that recycling preserves the ultrafast-to-early-nanosecond carrier dynamics without introducing additional defect-mediated recombination.

Preparing devices from recovered $MAPbI_3$

To compare the optoelectronic properties of films fabricated from recycled $MAPbI_3$ with those prepared from pristine $MAPbI_3$, we initially prepared simple photoconductor devices (Fig. 4a), enabling a direct comparison of bias-dependent dark and illuminated current density-voltage measurements.

The devices were illuminated using a 530 nm light source under varying illumination power and applied voltage, Fig. S16. Both sets of devices show a clear, monotonic increase in measured current density with increasing illumination intensity. The photocurrent density shows a strong dependence on light power. Interestingly the recycled films generate comparable current densities than the pristine counterparts at all illumination intensities. To visualize this difference more clearly, both types of devices were biased at 20 V and illuminated with an illumination intensity ranging from 2–25 mW cm^{-2}, while the corresponding current densities were recorded, Fig. 4b. The current density of the device prepared from the pristine $MAPbI_3$ increased from 0.13 $\times$ 10^{-5} to 0.7 $\times$ 10^{-5} A cm^{-2}, whereas the recycled device increased from 0.35 $\times$ 10^{-5} to 1.48 $\times$ 10^{-5} A cm^{-2}, suggesting a reduced defect density in the recycled film, consistent with the PL results. Subsequently, at 20 V, the dark current and light current densities of both devices were measured, Fig. 4c. The recycled films exhibit a dark current density (1.5 $\times$ 10^{-7} A cm^{-2}) that is slightly lower than the pristine film (2.4 $\times$ 10^{-7} A cm^{-2}). Overall devices prepared using recycled $MAPbI_3$ have comparable, arguably improved light-to-current performance than devices prepared from pristine $MAPbI_3$.

While photoconductors provide an excellent platform for evaluating the intrinsic optoelectronic properties of the recycled perovskite, the practical relevance of a recycling methodology ultimately depends on its compatibility with complete, multi-layer device architectures, in which multiple functional interfaces critically govern overall performance. To address this, full PV devices incorporating recycled $MAPbI_3$ were fabricated, Fig. 4d and benchmarked against pristine counterparts, Fig. 4e–h. The devices employed a p–i–n structure, comprising a solution-processed MeO-2PACz hole transport layer and a thermally evaporated C_{60}/BCP electron transport layer. The average PCEs of the pristine and recycled PSCs were 17.5 and 16.5%, respectively, with the recycled devices retaining 94% of the pristine PCE. This variation is primarily attributable to differences in fill factor, which is closely linked to interfacial quality. Notably, the box chart of PCE values for the recycled PSCs shows that some devices achieved efficiencies of up to 18%, comparable to the pristine counterparts.

Synthesis of perovskite nanocrystals using recovered $MAPbI_3$

To demonstrate the broader versatility of the solvent system, the $MAPbI_3$ recovered from thin films was successfully reused for the synthesis of perovskite nanocrystals (PNCs), extending the value of the recycled material beyond the original application. Perovskite thin films have had tremendous impact in light harvesting applications whereas PNCs have been utilised in light-emitting applications such as LEDs, Fig. 5a. Briefly, the recycled $MAPbI_3$ powder was dissolved in a solution of DMF

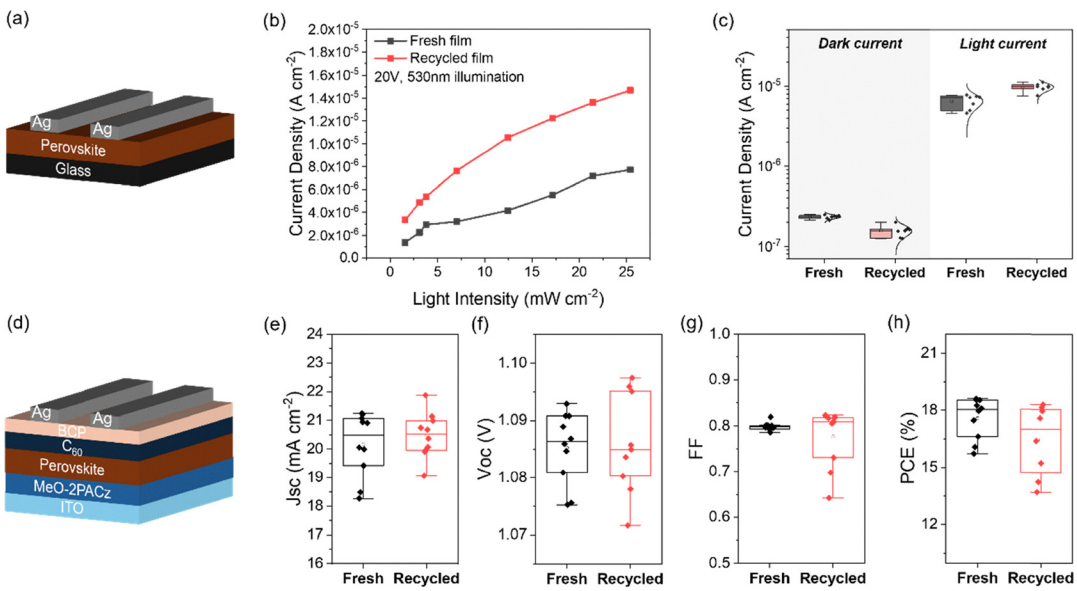


Fig. 4 (a) Schematic illustration of the photoconductor device structure. Photoconductor devices fabricated using fresh and recycled $MAPbI_3$ were characterised under 530 nm illumination. (b) Current density as a function of illumination intensity at an applied bias of 20 V, and (c) statistical comparison of the light and dark current densities, with the illuminated measurements obtained at 25.4 mW cm^{-2}. (d) Schematic illustration of the photovoltaic device structure. Statistical distributions of the key photovoltaic performance parameters for devices prepared using fresh and recycled $MAPbI_3$, presented as box-and-whisker plots: ((e) short-circuit current density (J_{sc}), (f) open-circuit voltage (V_{OC}), (g) fill factor (FF) and (h) power conversion efficiency (PCE).

containing oleic acid (OA) and oleylamine (OAm) at room temperature with vigorous stirring. This solution was then injected into chloroform resulting in the formation of PNCs, indicated by the red emission of the solution under 365 nm UV illumination, Fig. 5b.

TEM analysis revealed rod-shaped PNCs with average dimensions of approximately 18 nm along the short axis and 100 nm along the long axis, Fig. 5c. High-resolution TEM (HR-TEM) confirmed crystallinity, showing well-defined lattice fringes consistent with the (110) planes of tetragonal $MAPbI_3$.[54] This was further confirmed by XRD, which showed the tetragonal $MAPbI_3$ phase with the *I*4/*mcm* space group. Diffraction peaks at 14.2° and 28.5° 2θ correspond to the tetragonal (110) and (220) planes respectively, Fig. 5d. PNCs an additional resolved peak at 28.2° 2θ is seen, assigned to the (004) plane, indicating a different preferred crystal-growth orientation in the PNCs.[55] The full width at half maximum (FWHM) of the (110) peak at 14.23° also increased from 0.13° 2θ for the film to 0.22° 2θ for PNCs, consistent with a reduction in crystallite size.

The optical properties and stability of the PNCs were assessed by UV-vis absorption and PL spectroscopy. The PNC dispersion exhibited an absorption onset at approximately 750 nm and a PL emission maximum at 732 nm, with a FWHM of 55 nm, Fig. 5e. To evaluate colloidal stability, the PNCs were dispersed in chloroform, stored under ambient conditions, and their PL spectra recorded at 24 hour intervals, the integrated PL intensity being normalised to that of the freshly prepared dispersion. After 96 hours, the PNCs retained 81% of their initial PL intensity, indicating reasonable short-term stability, Fig. 5f. A progressive red-shift in the PL maximum was also observed, which is associated with the labile ligands, OA and OAm, that bind to the PNC surfaces dynamically.[56] Ligands desorption occurred during aging, leading to trap state formation and aggregation that produces a PL red-shift.[57,58]

The dimensions and optical properties of perovskite nanocrystals can be tuned by varying the ligand concentration and chain length.[59,60] The PNCs emitting at 732 nm therefore serve as a proof-of-concept demonstration that recycled $MAPbI_3$ powder can be repurposed as a luminescent nanomaterial.

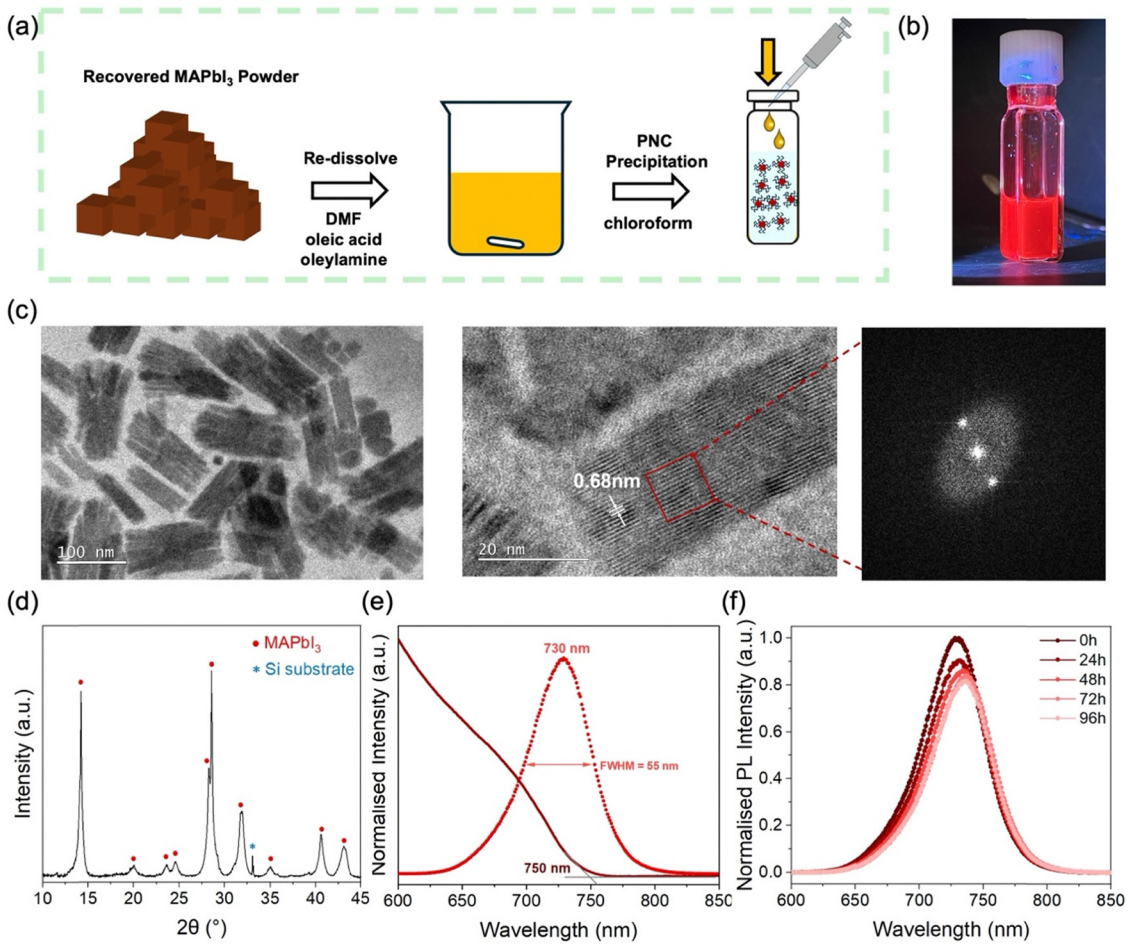


Fig. 5 Synthesis and characterisation of $MAPbI_3$ perovskite nanocrystals (PNCs) derived from recycled $MAPbI_3$ powder. (a) Schematic illustration of the PNC synthesis process. (b) Photograph of the resulting PNC dispersion under UV illumination. (c) TEM and HRTEM images of the PNCs with the corresponding electron diffraction pattern. (d) X-ray diffraction pattern of the $MAPbI_3$ PNCs. (e) UV-visible absorption and photoluminescence (PL) spectra of the PNC dispersion. (f) Normalised PL spectra recorded as a function of storage time.

 This journal is © The Royal Society of Chemistry 2026

This conversion of MHP films into emissive PNCs highlights the versatility of our recycling strategy, while reducing lead-containing waste and providing a potential route to functional materials for next-generation optoelectronic applications.

4. Conclusions

In summary, we have developed a green, efficient, and low-cost recycling strategy for $MAPbI_3$ thin films using an aqueous solvent system composed of malic acid, β-alanine, and sodium iodide. Combined FTIR, ^1H NMR, and Raman spectroscopy reveal that the dissolution mechanism relies on the formation of adducts between malic acid and lead species *via* Pb–carboxylate interactions, while the incorporation of NaI is critical to promote iodide-rich lead species in solution and ensure re-precipitation of $MAPbI_3$ rather than PbI_2, upon drying.

Thin films prepared from the recovered $MAPbI_3$ were compared with those prepared from fresh perovskite precursor solutions. The phase purity and elemental composition of recycled films show negligible differences from fresh perovskite films, with minor variations in XPS-derived C/N and Pb/I ratios attributable to known measurement artifacts (surface contamination and X-ray-induced reduction under vacuum) rather than intrinsic compositional differences. Films prepared from recycled $MAPbI_3$ exhibited slightly larger, more uniform grain sizes and a modestly longer average photoluminescence lifetime (18.7 ns *vs.* 16.8 ns) compared to fresh precursor films, the latter arising primarily from a redistribution in the relative amplitudes of the decay components rather than a change in the underlying carrier dynamics. These results indicate that performance is largely retained, rather than enhanced, through recycling.

Photoconductor devices prepared from recycled $MAPbI_3$ exhibited higher photocurrent and lower dark current compared to those fabricated from fresh $MAPbI_3$. To further validate device-relevant performance, full p–i–n photovoltaic devices incorporating recycled $MAPbI_3$—comprising a solution-processed MeO-2PACz hole transport layer and a thermally evaporated C_{60}/BCP electron transport layer—were fabricated and benchmarked against pristine counterparts. These devices achieved average power conversion efficiencies of 16.5% (recycled) *versus* 17.5% (pristine), retaining >90% of pristine performance, with select recycled devices reaching PCEs up to 18%, comparable to pristine analogues. This demonstrates that the recovered material remains fully compatible with complex, multi-interface device architectures without compromising performance. Additionally, the feasibility of producing high-quality rod-shaped perovskite nanocrystals from recycled powders further expands the application scope of our method, highlighting the versatility of the solvent system beyond thin-film reuse alone.

Overall, our approach offers a sustainable, low-cost, and scalable solution for lead recovery and $MAPbI_3$ reuse, demonstrating performance comparable to pristine materials across multiple structural, optoelectronic, and device-level metrics. This establishes a green and efficient route that supports a more circular lifecycle for emerging perovskite optoelectronic markets.

Conflicts of interest

There are no conflicts to declare.

Data availability

The data supporting the findings of this study are available in the supplementary information (SI) accompanying this article. Additional data requests can be made to the corresponding author upon reasonable request. Supplementary information is available. See DOI: https://doi.org/10.1039/d6mh01719c.

Acknowledgements

M. A. M., E. T. and M. S. P. S. gratefully acknowledge the EPSRC and SFI Centre for Doctoral Training in Advanced Characterisation of Materials (EP/S023259/1) for financial support. A. A. B. acknowledge funding from UKRI/EPSRC (ActionSpec, Grant Ref: EP/X030822/1). L. L. thanks Imperial College London for a President's PhD scholarship.

References

1 M. Li, Z. Zhu, Z. Wang, W. Pan, X. Cao, G. Wu and R. Chen, High-Quality Hybrid Perovskite Thin Films by Post-Treatment Technologies in Photovoltaic Applications, *Adv. Mater.*, 2024, **7**, 36.
2 Y. Liu, Z. Ma, J. Zhang, Y. He, J. Dai, X. Li, Z. Shi and L. Manna, Light-Emitting Diodes Based on Metal Halide Perovskite and Perovskite Related Nanocrystals, *Adv. Mater.*, 2025, **25**, 37.
3 Y. Mo, X. Huang, Q. Hu, C. Hu, P. K. Chu and J. Li, Recent progress in perovskite photodetectors: from carrier dynamics to device structures and applications, *Mater. Horiz.*, 2025, **18**(12), 7221–7243.
4 Y. Huang, Y. Feng, F. Li, F. Lin, Y. Wang, X. Chen and R. Xie, Sensing studies and applications based on metal halide perovskite materials: Current advances and future perspectives, *TrAC, Trends Anal. Chem.*, 2021, **134**, 116127.
5 R. Weiss, C. M. Sullivan and L. Nienhaus, Sizing Up Metal Halide Perovskite Photocatalysts: From Nano to Bulk, *Adv. Opt. Mater.*, 2024, **8**(12), 2300626.
6 C. Zou, Z. Ren, K. Hui, Z. Wang, Y. Fan, Y. Yang, B. Yuan, B. Zhao and D. Di, Electrically driven lasing from a dual-cavity perovskite device, *Nature*, 2025, **8080**(645), 369–374.
7 Y. Rong, Y. Hu, A. Mei, H. Tan, M. I. Saidaminov, S. Il Seok, M. D. McGehee, E. H. Sargent and H. Han, Challenges for commercializing perovskite solar cells, *Science*, 2018, **6408**, 361.
8 A. Sengupta, M. A. Afroz, B. Sharma, S. Choudhary, N. Pant, Y. Gulia, N. P. Kalapparambath Rajendra Pai, D. Angmo and S. Satapathi, Commercialization of perovskite solar cells:

opportunities and challenges, *Sustain. Energy Fuels*, 2025, **15**(9), 3999–4022.
9 P. Zhu, C. Chen, J. Dai, Y. Zhang, R. Mao, S. Chen, J. Huang and J. Zhu, Toward the Commercialization of Perovskite Solar Modules, *Adv. Mater.*, 2024, **15**, 36.
10 W. Zhang, H. Wang, Z. Chen and Y. Shao, Advancing the Commercialization of Perovskite-Based Radiation Detectors for High-Resolution Imaging, *Laser Photon. Rev.*, 2025, **5**(19), 2400470.
11 Y. Zhao, B. H. Choi, E. Kim, Q. Zeng and T. W. Lee, Advancing perovskite nanocrystals for high-resolution LED displays, *Commun. Mater.*, 2025, **1**(6), 281.
12 J. Yang, W. Wang, C. Bao, W. Huang and J. Wang, Toward practical applications of perovskite photodetectors: Advantages and challenges, *Matter*, 2025, **7**(8), 102207.
13 A. Babayigit, A. Ethirajan, M. Muller and B. Conings, Toxicity of organometal halide perovskite solar cells, *Nat. Mater.*, 2016, **3**(15), 247–251.
14 Unites States Environmental Protection Agency, Basic Information about Lead Air Pollution | US EPA, https://www.epa.gov/lead-air-pollution/basic-information-about-lead-air-pollution, (accessed 12 June 2026).
15 Z. Wu, M. Sytnyk, J. Zhang, G. Babayeva, C. Kupfer, J. Hu, S. Arnold, J. Hauch, C. Brabec and I. M. Peters, Closing the loop: recycling of $MAPbI_3$ perovskite solar cells, *Energy Environ. Sci.*, 2024, **12**(17), 4248–4262.
16 A. Binek, M. L. Petrus, N. Huber, H. Bristow, Y. Hu, T. Bein and P. Docampo, Recycling Perovskite Solar Cells To Avoid Lead Waste, *ACS Appl. Mater. Interfaces*, 2016, **20**(8), 12881–12886.
17 J. Roberto Bautista-Quijano, O. Telschow, F. Paulus and Y. Vaynzof, Solvent-antisolvent interactions in metal halide perovskites, *Chem. Commun.*, 2023, **59**, 10588.
18 T. Du, S. R. Ratnasingham, F. U. Kosasih, T. J. Macdonald, L. Mohan, A. Augurio, H. Ahli, C. T. Lin, S. Xu, W. Xu, R. Binions, C. Ducati, J. R. Durrant, J. Briscoe and M. A. McLachlan, Aerosol Assisted Solvent Treatment: A Universal Method for Performance and Stability Enhancements in Perovskite Solar Cells, *Adv. Energy Mater.*, 2021, **2101420**, 1–12.
19 F.-W. Liu, G. Biesold, M. Zhang, R. Lawless, J.-P. Correa-Baena, Y.-L. Chueh and Z. Lin, Recycling and recovery of perovskite solar cells, *Mater. Today*, 2021, **43**, 185–197.
20 B. Chen, C. Fei, S. Chen, H. Gu, X. Xiao and J. Huang, Recycling lead and transparent conductors from perovskite solar modules, *Nat. Commun.*, 2021, **1**(12), 5859.
21 Z. Du, J. Wei, D. Ding, M. Rimmele, Y. Dong, W. Qian, D. Nodari, F. Furlan, E. Angela, G. Morgan, P. Akinshin, W. R. Kazeem, G. Kerherve, A. V. Marsh, M. A. Isaacs, M. Heeney, T. J. Macdonald, S. A. Haque, N. Gasparini, D. Payne and M. McLachlan, Aqueous Preparation of CsPbBr3 Perovskite Nanocrystals Under Ambient Conditions, *Energy Environ. Sci.*, 2026, **19**, 5514–5526.
22 Z. Wu, M. Sytnyk, J. Zhang, G. Babayeva, C. Kupfer, J. Hu, S. Arnold, J. Hauch, C. Brabec and I. M. Peters, Closing the loop: recycling of MAPbI3 perovskite solar cells, *Energy Environ. Sci.*, 2024, **12**(17), 4248–4262.
23 X. Xiao, N. Xu, X. Tian, T. Zhang, B. Wang, X. Wang, Y. Xian, C. Lu, X. Ou, Y. Yan, L. Sun, F. You and F. Gao, Aqueous-based recycling of perovskite photovoltaics, *Nature*, 2025, **8051**(638), 670–675.
24 G. S. Shin, S. Kim, Y. Zhang and N. Park, A Correlation between Iodoplumbate and Photovoltaic Performance of Perovskite Solar Cells Observed by Precursor Solution Aging, *Small Methods*, 2020, **5**, 4.
25 E. Radicchi, F. Ambrosio, E. Mosconi, A. A. Alasmari, F. A. S. Alasmary and F. De Angelis, Combined Computational and Experimental Investigation on the Nature of Hydrated Iodoplumbate Complexes: Insights into the Dual Role of Water in Perovskite Precursor Solutions, *J. Phys. Chem. B*, 2020, **50**(124), 11481–11490.
26 T. Du, C. H. Burgess, J. Kim, J. Zhang, J. R. Durrant and M. A. McLachlan, Formation, location and beneficial role of PbI_2 in lead halide perovskite solar cells, *Sustain. Energy Fuels*, 2017, **1**, 119–126.
27 M. Szafrański and A. Katrusiak, Mechanism of Pressure-Induced Phase Transitions, Amorphization, and Absorption-Edge Shift in Photovoltaic Methylammonium Lead Iodide, *J. Phys. Chem. Lett.*, 2016, **17**(7), 3458–3466.
28 S. Rahimnejad, A. Kovalenko, S. M. Forés, C. Aranda and A. Guerrero, Coordination Chemistry Dictates the Structural Defects in Lead Halide Perovskites, *Chem. Phys. Chem.*, 2016, **18**(17), 2795–2798.
29 K. G. Stamplecoskie, J. S. Manser and P. V. Kamat, Dual nature of the excited state in organic–inorganic lead halide perovskites, *Energy Environ. Sci.*, 2015, **1**(8), 208–215.
30 O. Shargaieva, L. Kuske, J. Rappich, E. Unger and N. H. Nickel, Building Blocks of Hybrid Perovskites: A Photoluminescence Study of Lead-Iodide Solution Species, *Chem. Phys. Chem.*, 2020, **20**(21), 2327–2333.
31 C. Du, B. Liu, J. Hu and H. Li, Determination of iodine number of activated carbon by the method of ultraviolet–visible spectroscopy, *Mater. Lett.*, 2021, **285**, 129137.
32 X. Xiao, N. Xu, X. Tian, T. Zhang, B. Wang, X. Wang, Y. Xian, C. Lu, X. Ou, Y. Yan, L. Sun, F. You and F. Gao, Aqueous-based recycling of perovskite photovoltaics, *Nature*, 2025, **8051**(638), 670–675.
33 L. Wang, Y. Liu, X. Shu, S. Lu, X. Xie and Q. Shi, Complexation and conformation of lead ion with poly-γ-glutamic acid in soluble state, *PLoS One*, 2019, **9**(14), e0218742.
34 P. Pistor, A. Ruiz, A. Cabot and V. Izquierdo-Roca, Advanced Raman Spectroscopy of Methylammonium Lead Iodide: Development of a Non-destructive Characterisation Methodology, *Sci. Rep.*, 2016, **1**(6), 35973.
35 M. A. Pérez-Osorio, Q. Lin, R. T. Phillips, R. L. Milot, L. M. Herz, M. B. Johnston and F. Giustino, Raman Spectrum of the Organic–Inorganic Halide Perovskite $CH_3NH_3PbI_3$ from First Principles and High-Resolution Low-Temperature Raman Measurements, *J. Phys. Chem. C*, 2018, **38**(122), 21703–21717.
36 M. Nagai, T. Tomioka, M. Ashida, M. Hoyano, R. Akashi, Y. Yamada, T. Aharen and Y. Kanemitsu, Longitudinal Optical Phonons Modified by Organic Molecular Cation

 This journal is © The Royal Society of Chemistry 2026

Motions in Organic-Inorganic Hybrid Perovskites, *Phys. Rev. Lett.*, 2018, **14**(121), 145506.
37 C. Quarti, G. Grancini, E. Mosconi, P. Bruno, J. M. Ball, M. M. Lee, H. J. Snaith, A. Petrozza and F. De Angelis, The Raman Spectrum of the $CH_3NH_3PbI_3$ Hybrid Perovskite: Interplay of Theory and Experiment, *J. Phys. Chem. Lett.*, 2014, **2**(5), 279–284.
38 P. Pistor, A. Ruiz, A. Cabot and V. Izquierdo-Roca, Advanced Raman Spectroscopy of Methylammonium Lead Iodide: Development of a Non-destructive Characterisation Methodology, *Sci. Rep.*, 2016, **6**, 35973.
39 E. M. Nour and L. Shahada, Resonance Raman and far infrared spectroscopic studies of triiodide complexes formed in the reaction of iodine with some polycyclic amines, *Spectrochim. Acta, Part A*, 1989, **10**(45), 1033–1035.
40 W. M. Sears, M. L. Klein and J. A. Morrison, Polytypism and the vibrational properties of PbI2, *Phys. Rev. B:Condens. Matter Mater. Phys.*, 1979, **4**(19), 2305–2313.
41 V. Larini, C. Ding, B. Wang, R. Pallotta, F. Faini, L. Pancini, Z. Zhao, S. Cavalli, M. Degani, M. De Bastiani, F. Doria, C.-Q. Ma, F. You and G. Grancini, Circular management of perovskite solar cells using green solvents: from recycling and reuse of critical components to life cycle assessment, *EES Solar*, 2025, **3**(1), 378–390.
42 S. Moshat, J. Dhar, S. Sil and D. Sanyal, Positron annihilation spectroscopic studies of ferromagnetic methylammonium lead iodide perovskite, *J. Mater. Sci.*, 2024, **9**(59), 3919–3929.
43 C. Rocks, V. Svrcek, P. Maguire and D. Mariotti, Understanding surface chemistry during $MAPbI_3$ spray deposition and its effect on photovoltaic performance, *J. Mater. Chem. C*, 2017, **4**(5), 902–916.
44 A. García-Fernández, S. Svanström, C. M. Sterling, A. Gangan, A. Erbing, C. Kamal, T. Sloboda, B. Kammlander, G. J. Man, H. Rensmo, M. Odelius and U. B. Cappel, Experimental and Theoretical Core Level and Valence Band Analysis of Clean Perovskite Single Crystal Surfaces, *Small*, 2022, **13**, 18.
45 S. Ning, S. Zhang, J. Sun, C. Li, J. Zheng, Y. M. Khalifa, S. Zhou, J. Cao and Y. Wu, Ambient Pressure X-ray Photoelectron Spectroscopy Investigation of Thermally Stable Halide Perovskite Solar Cells via Post-Treatment, *ACS Appl. Mater. Interfaces*, 2020, **39**(12), 43705–43713.
46 S. Olthof and K. Meerholz, Substrate-dependent electronic structure and film formation of MAPbI3 perovskites, *Sci. Rep.*, 2017, **1**(7), 40267.
47 S. Wu, R. Chen, S. Zhang, B. H. Babu, Y. Yue, H. Zhu, Z. Yang, C. Chen, W. Chen, Y. Huang, S. Fang, T. Liu, L. Han and W. Chen, A chemically inert bismuth interlayer enhances long-term stability of inverted perovskite solar cells, *Nat. Commun.*, 2019, **1**(10), 1161.
48 A. L. Abdelhady, S. N. Afraj, Y. Haruta, M. M. Uddin and M. I. Saidaminov, Metallic Lead Formation in Perovskites: Mechanisms, Suppression, and Future Directions, *ACS Nano*, 2025, **40**(19), 35276–35305.
49 M. De Keersmaecker, P. Dietrich, M. Bahri, N. D. Browning, N. R. Armstrong and E. L. Ratcliff, Activated Corrosion and Recovery in Lead Mixed-Halide Perovskites Revealed by Dynamic Near-Ambient Pressure X-ray Photoelectron Spectroscopy, *J. Am. Chem. Soc.*, 2025, **10**(147), 8881–8892.
50 W.-C. Lin, W.-C. Lo, J.-X. Li, Y.-K. Wang, J.-F. Tang and Z.-Y. Fong, In situ XPS investigation of the X-ray-triggered decomposition of perovskites in ultrahigh vacuum condition, *Npj Mater. Degrad.*, 2021, **1**(5), 13.
51 P. Zhu, D. Wang, Y. Zhang, Z. Liang, J. Li, J. Zeng, J. Zhang, Y. Xu, S. Wu, Z. Liu, X. Zhou, B. Hu, F. He, L. Zhang, X. Pan, X. Wang, N.-G. Park and B. Xu, Aqueous synthesis of perovskite precursors for highly efficient perovskite solar cells, *Science*, 2024, **6682**(383), 524–531.
52 D. W. de Quilettes, S. M. Vorpahl, S. D. Stranks, H. Nagaoka, G. E. Eperon, M. E. Ziffer, H. J. Snaith and D. S. Ginger, Impact of microstructure on local carrier lifetime in perovskite solar cells, *Science*, 2015, **6235**(348), 683–686.
53 W. Shao, H. Wang, S. Fu, Y. Ge, H. Guan, C. Wang, C. Wang, T. Wang, W. Ke and G. Fang, Tailoring Perovskite Surface Potential and Chelation Advances Efficient Solar Cells, *Adv. Mater.*, 2024, **24**, 36.
54 T. Wang, S. Hou, H. Zhang, Y. Yang, W. Xu, T. Ao, M. Kang, G. Pan and Y. Mao, Highly controllable synthesis of MAPbI3 perovskite nanocrystals with long carrier lifetimes and narrow band gap for application in photodetectors, *J. Alloys Compd.*, 2021, **872**, 159589.
55 L. A. Muscarella, E. M. Hutter, S. Sanchez, C. D. Dieleman, T. J. Savenije, A. Hagfeldt, M. Saliba and B. Ehrler, Crystal Orientation and Grain Size: Do They Determine Optoelectronic Properties of $MAPbI_3$ Perovskite?, *J. Phys. Chem. Lett.*, 2019, **20**(10), 6010–6018.
56 J. De Roo, M. Ibáñez, P. Geiregat, G. Nedelcu, W. Walravens, J. Maes, J. C. Martins, I. Van Driessche, M. V. Kovalenko and Z. Hens, Highly Dynamic Ligand Binding and Light Absorption Coefficient of Cesium Lead Bromide Perovskite Nanocrystals, *ACS Nano*, 2016, **2**(10), 2071–2081.
57 T. K. T. Tran, H. N. Nyiera and J. Zhao, Instability of colloidal lead halide perovskite nanocrystals: Causes, improvement, and evaluation, *Nano Res.*, 2024, **12**(17), 10607–10619.
58 H. Shankar, W. W. Yu, Y. Kang and P. Kar, Significant boost of the stability and PLQYof CsPbBr3 NCs by Cu-BTC MOF, *Sci. Rep.*, 2022, **1**(12), 7848.
59 J. Cho, Y.-H. Choi, T. E. O'Loughlin, L. De Jesus and S. Banerjee, Ligand-Mediated Modulation of Layer Thicknesses of Perovskite Methylammonium Lead Bromide Nanoplatelets, *Chem. Mater.*, 2016, **19**(28), 6909–6916.
60 S. Kumar, J. Jagielski, S. Yakunin, P. Rice, Y.-C. Chiu, M. Wang, G. Nedelcu, Y. Kim, S. Lin, E. J. G. Santos, M. V. Kovalenko and C.-J. Shih, Efficient Blue Electroluminescence Using Quantum-Confined Two-Dimensional Perovskites, *ACS Nano*, 2016, **10**(10), 9720–9729.